remote sensing

MDPI

Article

Relationship of Attributes of Soil and Topography with Land Cover Change in the Rift Valley Basin of Ethiopia

Gebiaw T. Ayele [1], Ayalkibet M. Seka [2], Habitamu Taddese [3], Mengistu A. Jemberrie [4], Christopher E. Ndehedehe [1], Solomon S. Demissie [5], Joseph L. Awange [6], Jaehak Jeong [7], David P. Hamilton [1] and Assefa M. Melesse [8,*]

1 Australian Rivers Institute and School of Engineering and Built Environment, Griffith University, Nathan, QLD 4111, Australia; gebiaw.ayele@griffithuni.edu.au (G.T.A.); c.ndehedehe@griffith.edu.au (C.E.N.); david.p.hamilton@griffith.edu.au (D.P.H.)
2 Key Laboratory of Digital Earth Science, Aerospace Information Research Institute, Chinese Academy of Sciences, Beijing 100094, China; aabmdb.seka4@mails.ucas.edu.cn
3 Wondo Genet College of Forestry and Natural Resources, Hawassa University, Shashemene P.O. Box 128, Ethiopia; habitamu@hu.edu.et
4 School of Civil Engineering and Architecture, Adama Science and Technology University, Adama P.O. Box 1888, Ethiopia; mengistu.addis@astu.edu.et
5 Civil & Environmental Engineering Department, University of California, 6722 Boelter Hall, 420 Westwood Plaza, Los Angeles, CA 90095, USA; solomon.seyoum@aau.edu.et
6 Department of Earth and Planetary Sciences, Spatial Sciences, Curtin University, Perth, WA 6845, Australia; j.awange@curtin.edu.au
7 Blackland Research & Extension Center, Texas A&M AgriLife Research, 720 East Blackland Rd, Temple, TX 76502, USA; jaehak.jeong@brc.tamus.edu
8 Department of Earth and Environment, Florida International University, Miami, FL 33199, USA
* Correspondence: melessea@fiu.edu

Abstract: Understanding the spatiotemporal trend of land cover (LC) change and its impact on humans and the environment is essential for decision making and ecosystem conservation. Land degradation generally accelerates overland flow, reducing soil moisture and base flow recharge, and increasing sediment erosion and transport, thereby affecting the entire basin hydrology. In this study, we analyzed watershed-scale processes in the study area, where agriculture and natural shrub land are the dominant LCs. The objective of this study was to assess the time series and spatial patterns of LCC using remotely-sensed data from 1973 to 2018, for which we used six snapshots of satellite images. The LC distribution in relation to watershed characteristics such as topography and soils was also evaluated. For LCC detection analysis, we used Landsat datasets accessed from the United States Geological Survey (USGS) archive, which were processed using remote sensing and Geographic Information System (GIS) techniques. Using these data, four major LC types were identified. The findings of an LC with an overall accuracy above 90% indicates that the area experienced an increase in agricultural LC at the expense of other LC types such as bushland, grazing land, and mixed forest, which attests to the semi-continuous nature of deforestation between 1973 and 2018. In 1973, agricultural land covered only 10% of the watershed, which later expanded to 48.4% in 2018. Bush, forest, and grazing land types, which accounted for 59.7%, 16.7%, and 13.5% of the watershed in 1973, were reduced to 45.2%, 2.3%, and 4.1%, respectively in 2018. As a result, portions of land areas, which had once been covered by pasture, bush, and forest in 1973, were identified as mixed agricultural systems in 2018. Moreover, spatial variability and distribution in LCC is significantly affected by soil type, fertility, and slope. The findings showed the need to reconsider land-use decision tradeoffs between social, economic, and environmental demands.

Keywords: GIS and remote sensing; spatiotemporal modelling; image processing; land cover change detection; soil spatial variability; soil–land use–slope interaction; kriging

Citation: Ayele, G.T.; Seka, A.M.; Taddese, H.; Jemberrie, M.A.; Ndehedehe, C.E.; Demissie, S.S.; Awange, J.L.; Jeong, J.; Hamilton, D.P.; Melesse, A.M. Relationship of Attributes of Soil and Topography with Land Cover Change in the Rift Valley Basin of Ethiopia. *Remote Sens.* **2022**, *14*, 3257. https://doi.org/10.3390/rs14143257

Academic Editor: Frédérique Seyler

Received: 5 May 2022
Accepted: 4 July 2022
Published: 6 July 2022

1. Introduction

The conversion of land cover (LC) has occurred for millennia and has intensified with population increase on a globally significant scale over recent decades [1]. Land cover change (LCC) is driven by interactions between socioeconomic activities, institutional and environmental factors, human population density, vegetation cover, and climatic conditions [2,3]. For example, urban areas have expanded in response to population growth and economic development with encroachment on agricultural and untouched areas [4]. LCC has therefore become a key research priority for national and international research programs examining local and global environmental change [5,6].

Change in LC (e.g., forest to bare land) alters the fluxes of water and sediment leading to reduced soil moisture content and base flow, accelerated overland flow, and increased soil erosion and the widespread degradation of watersheds [7]. In this regard, various studies have used LC mapping tools and methods to understand LCCs and the changes in the hydrologic behavior of watersheds [8–12].

There have been dramatic LCCs throughout Ethiopia over the last few decades, where forest cover in highland areas has decreased from more than 90% to less than 4% [13]. This change has influenced diverse aquatic and terrestrial resources including the Blue Nile [14]. The change is thought to be linked to increases in population and the resulting degradation of natural resources and loss of biodiversity. Elias et al. [14] reported that rates of natural resource degradation and biodiversity loss showed a marked increase in the last five decades of the 20th century, associated with changes in LC and leading to the deterioration in water quality in rivers and lakes (e.g., Awash River, Lake Abaya, and Lake Ziway). Other studies [5,15] have emphasized that changes in LC can adversely affect the quality of life and human wellbeing.

The Ethiopian Rift Valley basin has undergone major changes in LC due to population and agricultural expansion, which includes floriculture and irrigated cropland [16,17]. For instance, in an LCC study conducted on the Central Rift Valley of Ethiopia, [18] found that between 1973 and 2014, agricultural areas expanded at the expense of all other LC types. According to their findings, during this period, the rate and magnitude of LCC for each of the four major LC types: water, forest, grass, and woodland, declined by 3%, 6%, 13%, and 15%, respectively, concurrently with a 36% increase in agricultural area. A similar study in the basin [16] supports the findings of [18], and it highlighted that LCC is one of the phenomena that interweaves with the socioeconomic and environmental status in the area and the country at large. As a result, estimating temporal patterns and the magnitude and trends in LCC at the watershed, basin, and regional scales [19] can provide valuable information on the expected extent of change in water resources and socioecological responses.

Previous studies on the spatial variability in soil and LC are either site-specific, coarse-scale (e.g., basin scale studies), or implemented pedo-transfer functions (PTFs) that neither provide all the required data inputs nor account for environmental effects [20–22]. This means that no significant research in the region has followed a bottom-up approach to drive the LC and soil–topography relationship and upscale the result for hydrological modelling. In addition, the region lacks research that can associate subbasin scale spatiotemporal LCC with watershed characteristics including topography and soils. It should also be pointed out that the accurate LCC predictions and assessments of soil fertility, hydrological cycles, biodiversity, biogeochemical cycles, and energy balances are only accurate at the smaller spatial scales, i.e., from the plot to watershed level [23]. Fine-scale assessments of the spatiotemporal watershed soil and LC status and its rate of change in Ethiopia is therefore paramount to support the development of environmental protection and sustainability plans [17].

This research, on the other hand, assesses the spatial dynamics of LC and soil properties to understand time series LCC and landscape physicochemical processes in the area. The significance of the work, therefore, stems from three aspects. Firstly, we reconstructed historical LC data, mapped soil–topography–LC interactions, and performed change de-

tection analysis; secondly, from the fact that, in our research, we did not rely using either the coarse resolution FAO soils guidelines that assign the same soil property at different landscape gradients or site-specific and unreliable PTFs. Instead, we performed a detailed field survey and laboratory analysis and developed the soil–landscape relation for a tropical catchment in the Rift Valley basin where data are scarce resources. Thirdly, by using catchment hydrological characterization using fine-scale soils, time series remotely-sensed data, and historical runoff data, the study can provide a reference for the rational allocation of water resources and the adjustment of land use structure for decision makers.

Furthering the significance of our research, the implications of LCC on the environment have been reported. For example, [24] highlighted that soil physical attributes are highly related to topography and changes in soil properties can affect the soil's water content, vegetation response, and the rate and intensity of LCC [25]. The relationship between watershed soil properties and topography and how they interact with changes in LC in areas identified with high topographic heterogeneity is also documented [26]. It is also argued that soil type affects moisture retention, which is a major mechanism for influencing LC [26]. Therefore, the assessment of the soil–topography effects on LC distribution requires reliable LC information that is generated based on systematic methods, tools, and techniques [27]. The LC information of the area was extracted using the maximum likelihood classification (MLC) algorithm for supervised classification [28].

Following the LC classification, various approaches have been proposed to assess LCC detection [29]. In this study, we implemented object-based MLC as it is one of the most widely used and robust supervised training algorithms [30]. For example, [30] used an object-based MLC technique for LCC detection as it overcame some of the particular problems encountered with pixel-based classification.

The overarching aim of this study was to determine the rate and magnitude of LCC in the Batena watershed during the period of 1973–2018. The specific objectives were to (i) assess the time series LCC and perform change detection analysis between 1973 and 2018 and (ii) evaluate the pattern, rate, trend, and magnitude of long-term spatiotemporal LCC. It also aimed to characterize the effect of soil and topography on LC distribution, spatially correlate soil properties and topographic attributes, and assess the interactive effect of soil, LC type, and slope position on soil physicochemical properties.

To achieve this, we examined the time series and spatial patterns of LCC using change detection methods applied over the catchment between 1973 and 2018. We used satellite images and the Environment for Visualizing Images (ENVI) software to assess the trend of LCC [31,32]. Multi-temporal Landsat products provided the opportunity to distinguish LC types by employing change detection analysis at various time points [33]. Consequently, we used the historical Landsat datasets [29], applied a Bayesian MLC algorithm to assess the different LC types [34,35], and used change detection comparison techniques to identify intra-image LCC [36]. Grid scheme field observations and discussions with local people were also employed to validate results from remotely-sensed data. Based on the results of field observation, four major LC types were identified in the watershed, and changes in each class were identified.

2. Materials and Methods

2.1. Study Area

The Batena watershed (117 km^2) in the Rift Valley lakes basin drains into Bilate River on its way to Lake Abaya. The area is located in the rural mountainous part of the Rift Valley lakes basin, southwestern part of Ethiopia (Figure 1) between 7.4° and 7.72°N latitude, and 37.8° and 37.9°E longitude. The topography of the area has two distinct features: rugged mountainous highland areas in the northern and northwestern part of the watershed and lowlands in the eastern watershed. The area lies at altitudes ranging from 2065 m to 2947 m above mean sea level. The region is characterized by steep to moderate hilly slopes and the two clay rich soils found in this slope range are chromic, pellic vertisols and chromic luvisols. Cultivated land is common at all altitudinal ranges. Apart from agricultural

lands, the study landscape comprises mosaics of mixed forests, grazing land, and bushland. Built-up areas are sparse and small and were not represented in our analysis. Bilate river basin, which includes this watershed, has alluvial sediments of gravel, sand, and clay with pedogenetic profiles sloping smoothly to the bed [37].

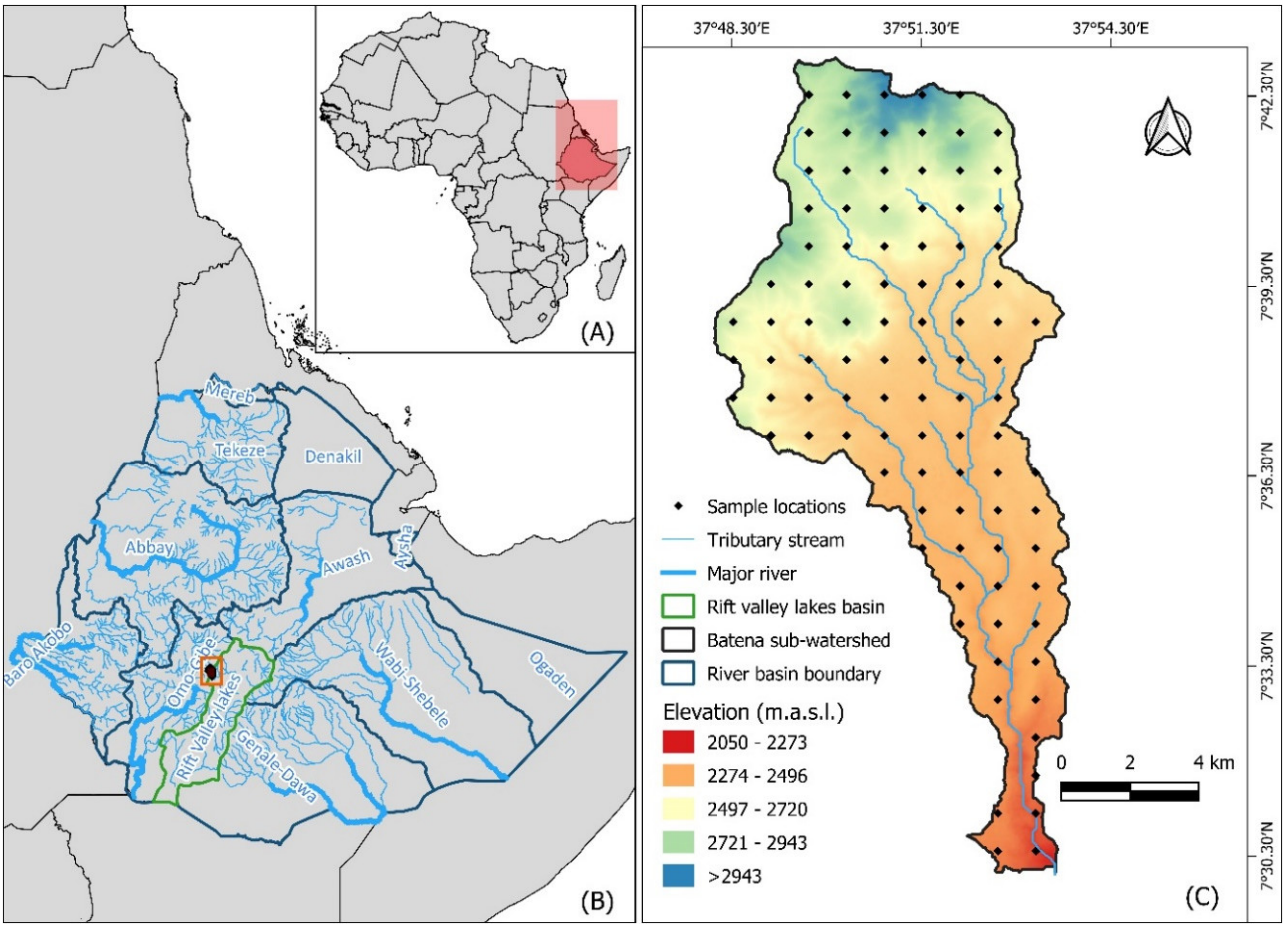

Figure 1. Location of Ethiopia in Africa (**A**), Batena watershed in the Rift Valley basin (**B**), and Batena watershed (**C**). Elevation classes 1–5 indicate altitudinal gradients in increasing order.

The climate of the region is mainly controlled by seasonal migration of the Intertropical Convergence Zone (ITCZ) and its associated atmospheric circulation. Annual rainfall ranges between 1280 mm and 1339 mm, and the annual mean minimum and maximum temperature varied from 11 °C to 22 °C, respectively, based on local weather station data [7].

2.2. Methodology

2.2.1. Datasets

To assess the rate and magnitude of LCC, a series of multi-sensor Landsat images were accessed from the USGS data portal (https://earthexplorer.usgs.gov; accessed on 20 March 2020) (Table 1). They included acquisition of medium resolution Landsat satellite data: Multi-spectral Scanner System (MSS), Thematic Mapper (TM), Landsat-7 Enhanced Thematic Mapper Plus (ETM+) [38], and Landsat-8 OLI (Operational Land Imager) in a regular and tiled fashion following the World Reference Systems (WRS1 for MSS, WRS2 for TM, ETM+, and Landsat 8). The data spanned nearly five decades and used MSS for the 1970s, TM for the 1980s and 1990s, ETM+ for 2000s, and Landsat 8 OLI for the 2010s. A digital elevation model (DEM) of the area with 30 m horizontal vertical resolution was obtained from the Ethiopian Ministry of Water and Energy, GIS and remote sensing department.

Table 1. Summary of the characteristics of Landsat images used in this study (1973–2018).

Sensor Type	Date of Acquisition	Path	Row	Spatial Resolution (m)	Temporal Resolution (Days)
MSS	31 January 1973	181	55	60	18
TM	22 November 1984	169	55	30	16
TM	21 January 1995	169	55	30	16
ETM+	24 November 2003	169	55	30	16
ETM+	27 November 2008	169	55	30	16
OLI	20 November 2018	169	55	30	16

Source: United States Geological Survey, USGS (https://earthexplorer.usgs.gov/, accessed on 20 March 2020).

Different kinds of satellite images and ancillary datasets were collated to identify historical and recent LC information and seasonal development of vegetation manifested (Table 1). The oldest available dataset used Landsat MSS archive at the EROS Data Center. These datasets obtained from the Global Land Cover Facility (GLCF) were taken by Landsat 1 (ESAT1) on 31 January 1973 at WRS1 path 181 and row 55. The satellite that carries the MSS instrument on board, Landsat 1, orbited at 920 km height with 18 days repeat cycle. The image data from MSS consists of four spectral bands covering the visible green, red, and two near-infrared wavelengths.

The TM and ETM+ sensors are designed to achieve sharper spectral separation, higher image resolution, greater radiometric accuracy and resolution, and improved geometric fidelity than the MSS sensor. These sensors have a 30 m spatial resolution for bands 1–5, and band 7, and a 120 m or 60 m resolution for band 6 for TM and ETM+, respectively. A single scene covering 169/55 (path/row) was taken on November 1984 using TM sensor on board Landsat 5. The same path/row image taken in January 1995 was employed to assess the decadal LC at 30 m spatial resolution ETM+, and Landsat 8 OLI datasets taken on November 2003, 2008, and 2018 were also used in the time series LC and change detection analysis.

2.2.2. Image Processing

Digital image processing involved manipulation and interpretation of digital images using pre-processing, enhancement, transformation, classification, and analysis functions. Pre-processing comprises a series of sequential operations, including atmospheric correction, image registration, normalization, geometric correction, and masking. We checked that these had already been implemented from the source. Prior to image classification, spatial resolution of the images (MSS, TM, ETM+, and Landsat 8 OLI) was enhanced by using resolution merge technique that integrates images of different spatial resolution. Stripping and banding errors were accounted for through radiometric enhancement [38,39]. Principal component analysis (PCA), on the other hand, improved the image visualization with a technique of data compression to segregate noise components and reduce the dimensionality of datasets, and produce uncorrelated output bands [40].

The methodology employed in the LC assessment included image interpretation, preliminary LC classification and mapping, and post-classification tasks (Figure 2). Geometric and radiometric corrections were applied to reduce geospatial data uncertainty resulting from image resampling, percent cloud cover, and assumptions of homogeneity [41]. During image processing, color balance was used for image enhancement through histogram equalization [23], and radiometric correction was undertaken to minimize the effect of atmospheric factors.

Supervised image classification was used to create time series land cover data of the watershed. Training data were collected during the soil sampling fieldwork. The dominant land cover classes identified in this study were agriculture, bushland, grazing land, and mixed forest. The other small patches of land cover such as built-up areas were neglected due to their insignificant contribution to the watershed area. Those training sample data were used to train the algorithm and generate sample statistics, which were

used for supervised classification. The MLC, maximum likelihood classification, algorithm was used to classify unsampled pixels into the target classes of land cover included in the training process. ENVI software was used to run the image classification.

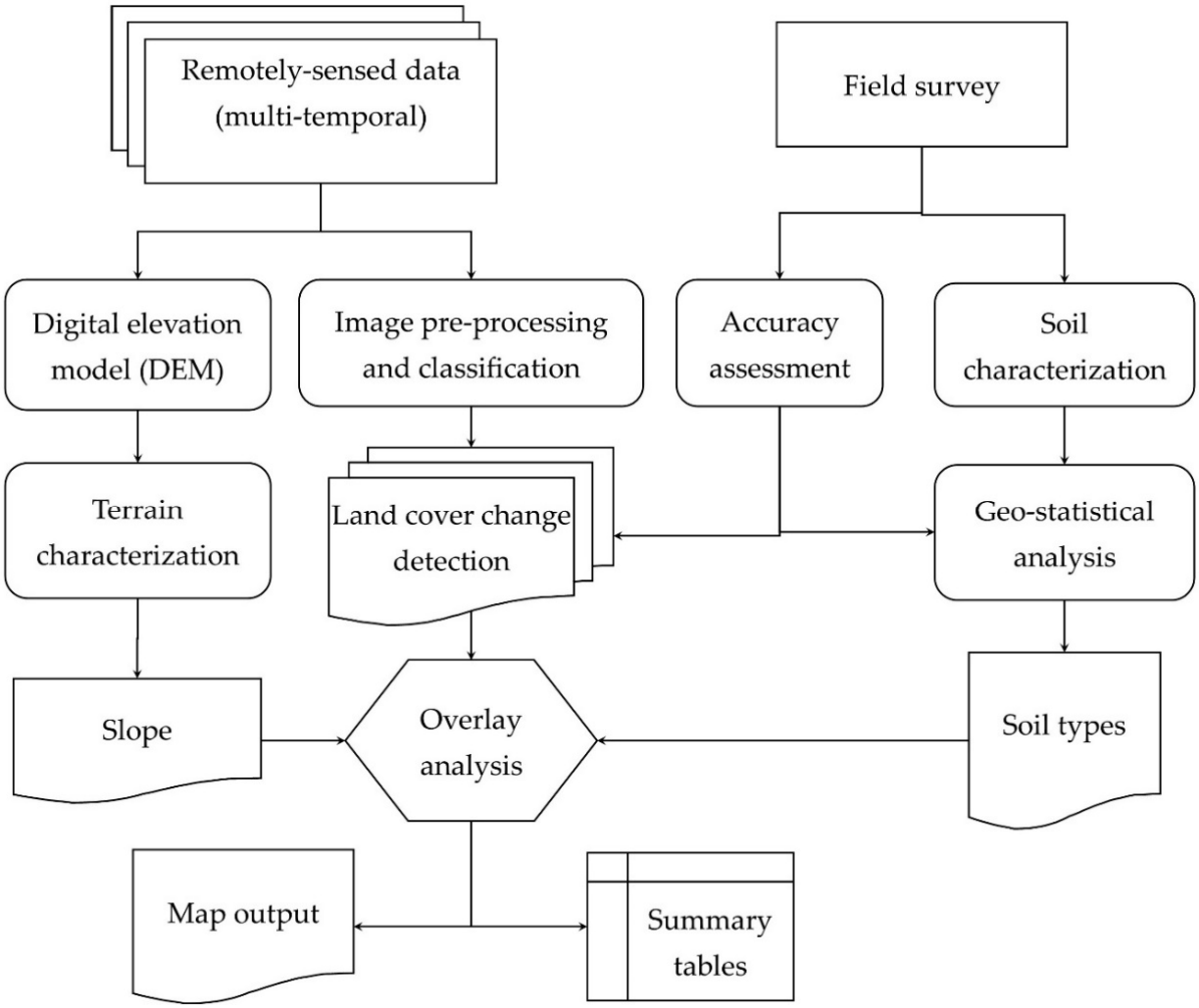

Figure 2. The study workflow in which image and field survey data collection and analysis steps are depicted. The angular rectangles represent the data sources (i.e., remote sensing and field survey); round edged rectangles mean the different individual analysis methods; the hexagonal symbol represents the overlay operation, which integrated the different data types; the trapezium-shaped symbol that has one irregular side represents the image output, while the table frame represents tabular output.

For LCC analysis with different dates of acquisition, images were resampled to a higher spatial resolution, layer stacked, and geometrically transformed before use for analysis. Geometric transformation of digital images modified the spatial relationship between pixels in an image for post-processing. Conversion of satellite image from fine-scale to a coarser spatial resolution with images from similar or different satellite sensors of varying spatial resolutions involves image resampling. The choice of resampling method depends, among others, on the ratio between input and output pixel size and the purpose of resampled images [42]. In this research, the Landsat Multispectral Scanner image of 1973 with a pixel size of 60 × 60 m was resampled into a pixel size of 30 × 30 m using the nearest neighbor method to preserve the original image radiometric information [42–44].

2.2.3. Land Cover Change Detection

Many techniques have been developed to assess LCC between images of varying dates [45], such as conventional image differentiation, image regression, image ratio, manual on-screen digitization of change, principal components analysis, multi-date image classification, and post-classification comparison [46]. Of these classification methods, post-classification comparison that uses ML object-based classification technique that gained prominence in the field of remote sensing was principally employed [30]. The study findings of [30] and the references therein indicate that object-based image analysis involves image segmentation that partitions images into homogeneous and non-overlapping regions that are later identified as objects. It is also suggested that object-based classification is recommended as it overcomes some of the particular problems (e.g., disregarding geometric and contextual information) encountered with pixel-based classification [29]. In addition, in object-based image analysis, a range of diagnostic features for a specific object can be integrated on the basis of expert knowledge, and it aims to represent the content of a complex scene in a manner that best describes the imaged reality by mimicking human perception. The other advantage of object-based image classification is that, by the incorporation of textural data, spatial characteristics, and spectral information, it approaches the way that humans visually interpret the information on satellite images and aerial photos. During ML classification, image data were first classified by aggregating images into scene clusters based on their inherent spectral properties and local area knowledge of LC types, which were used to develop training site for supervised classification.

LC classification was defined according to the classification schemes in FAO guidelines [47] where LC of the area was mapped using vegetation cover, type, and intensity of cultivation. Following image post-processing through MLC, change detection was used to quantify the rate, magnitude, and pattern of change [48]. Of the various change detection comparison procedures [49], post-classification comparison was applied to identify intra-image LCC. This technique compares classifications of initial and final state images to identify intra-image LCC. According to [49], for example, post-classification comparison was the most accurate procedure.

Extending the analysis of trend and intensity of LCC, we used two indicators that characterize LCC: LCC intensity index (LCI) and vegetation change index (VCI). LCI was used to assess the intensity of LCC. The higher the absolute value of LCI for a specific LC type, the more intense the LCC in the watershed and vice versa. For each LC type considered, the value of LCI was calculated as the area of LCC divided by total watershed area (Equation (1))

$$LCI_i = \frac{a_i}{A} * 100\% \quad (1)$$

where LCI_i is the LCC intensity index ranging from 0 to 1; a_i is change in area of LC type i in km^2; A is the total watershed area in km^2.

The other important factor used to quantify the intensity of LCC and degree of vegetation restoration was the VCI (Equation (2)). VCI indicates the change in area of vegetation (i.e., numerical sum of forest, shrub, medium, and high-coverage grassland) obtained from time series LC maps. VCI values greater than zero show an increase in vegetation cover and those less than 0 indicate a decrease in vegetation cover with a value of zero representing unchanged vegetation cover.

$$VCI = R_2 - R_1 \quad (2)$$

where R_1 and R_2 represent the initial and final vegetation cover in percent, respectively.

2.3. Accuracy Assessment

Prior to implementation of the error matrix approach to assess classification accuracy [50], we collected validation samples at all soil sampling points that were performed in a grid scheme (see Figure 1, Section 3.2.2). In addition, LC training samples were collected in areas where we identified different LC types. Error matrix was used to compare ground truth data with the classified LC types for all satellite images (MSS 1973, TM 1984, TM

1995, ETM + 2003, ETM+ 2008, and OLI 2018). It was also used to provide a detailed assessment of the agreement between classified results and the reference data obtained in the field observations.

The accuracy of image classification was carried out using a confusion matrix generated through GIS overlay of the classified maps and test samples. The measure of overall accuracy is obtained by dividing the total number of correctly classified samples by the total number of samples in the error matrix. The possible bias towards the LC category with a larger number of samples was addressed by representative reference data points. The image classification accuracy was further assessed by calculating the Kappa coefficient ($\hat{k}$), an estimate of overall agreement between image and the ground truth data with values of $\hat{k}$ ranging between 0 and 1 [51]. A $\hat{k}$ value of 0 indicates no agreement between two tests, while a value of 1 shows a perfect agreement. $\hat{k}$ is often multiplied by 100 to give a percentage measure of classification accuracy. $\hat{k}$ values are also characterized into three groupings: a value greater than 0.8 for strong agreement, a value between 0.4 and 0.8 for moderate agreement, and below 0.4 representing poor agreement [50,52]. $\hat{k}$ can be negative indicating the level of agreement is less than would be expected just by chance.

$$\hat{k} = \frac{N\sum_{i=1}^{r} X_{ii} - \sum_{i=1}^{r} X_{i+}X_{+i}}{N^2 - \sum_{i=1}^{r} X_{i+}X_{+i}} = \frac{\theta_1 - \theta_2}{1 - \theta_2} \quad (3)$$

$$\theta_1 = \sum_{i=1}^{r} \frac{X_{ii}}{N} \text{ and } \theta_2 = \sum_{i=1}^{r} \frac{X_{i+}X_{+i}}{N^2} \quad (4)$$

where X_{i+} is the sum of the ith row, X_{+i} is the sum of the ith column, and X_{ii} is the count of observations at row i and column i, r is the number of rows or columns in the error matrix, while N is the total number of observations in the error matrix.

2.4. Soil, Topography, and Land Cover Characterization

2.4.1. Soil Survey and Mapping

A combination of field and laboratory work was used to identify the relation between LC and basic soil physicochemical properties. Such data were also used to establish the distribution of soils for assessing land capability. Soil samples were collected from systematically aligned 97 field plots (1 plot for each 1 km^2 grid) by using soil sample pits and description augers. Soil field survey and mapping followed the latest United States Department of Agriculture natural resource conservation service norms and standards for field mapping [53].

Through soil sampling, it was possible to estimate and characterize LC and soil physical and chemical attributes at non-sampled sites through existing models. However, because of the highly complex relationship among the unpredictable spatial patterns and sampled soil spatial properties [54], implementation of probabilistic method admits some uncertainty on the spatial variation and soil properties at the unmeasured sites; these are considered to be outcomes of some random process [55], which are not achieved through the deterministic method of soil characterization.

The surface map was built using Kriging (point iterations), which estimates the statistical relationships among the sample points with the assumption that the distance between sampling points reflects a spatial correlation that can be used to explain data variations [56]. The model first creates an empirical semi-variogram representing the variance for each pair of observation points followed by adjustment of the model to fit the semi-variogram. The methodology adopted in this study is presented in Figure 2, explaining how LC and soils are mapped prior to assessing soil–LC–slope interactions.

For soil mapping, we implemented geostatistical analysis that elucidates soil spatial pattern within the area and allows interpolation of soil variables to unmeasured locations throughout the landscape using the variogram model in kriging. Variogram modeling is an advanced geostatistical tool that generates an estimated surface from a scattered set of points with z-values. Soil property prediction maps were created using a set of

training data as input to Kriging point iteration, which works with the regionalized variable theory [57]. The spatial variation is estimated using semi-variogram [58] computed from soil samples collected from field and laboratory across the study area that followed a gridded sampling scheme [56].

2.4.2. Relationship of Soil, Topography, and Land Cover

Soil sampling plot locations (at elevations between 2065 and 2947 m. a. s. l.) were identified based on the LC map in a grid scheme (Section 3.2.1). Individual sampling locations were chosen in such a way that pairs of composite soil samples (soil pits and description augers) were taken at adjacent places in the same geomorphologic setting and different LC types. This technique of sampling minimizes the pedogenetic variability in the sampled soil [59]. In addition, informal interviews were held with the local community to find out the cultivation period of each cultivated land to determine its impact on soil physicochemical properties such as soil organic carbon [60,61]. In summary, a detailed soil survey and onsite LC validation were performed in order to identify the relation between terrain slope, LC, and soil type.

In furthering the soil–LC–terrain characterization, the magnitude and pattern of soil's physical and chemical attributes were mapped using the FAO [47] guidelines. As a result of the complex slope–LC relationships among soil properties and the unpredictable spatial pattern [54], deterministic method of soil characterization does not result in accurate estimation. Probabilistic methods, on the other hand, show some uncertainty about how soil properties could vary in space, and soil properties at the unmeasured sites are considered to be outcomes of some random process [55]. In this regard, we used a class of geostatistical technique to assess terrain–LC effects on the spatial distribution of soil properties. This method provides a wide variety of tools for identification of data anomalies, spatial data exploration, evaluation of errors in prediction of surface models, and creation of statistical estimation and optimal surfaces [62]. Kriging point iteration technique was used to create prediction maps from field training datasets and laboratory analysis results [57].

3. Results and Discussion

3.1. Land Cover Change

Regarding the field survey and the output of the Landsat image analysis, the final Bayesian ML classification resulted in four major LC types with automatic merging of the closer values of reflectance properties and characteristics. The LC maps of the study area for the six reference years (Figure 3a, Table 2) indicated that only about 23.5% of the watershed was under cultivation and grazing in 1973, while the remaining 76.5% was predominantly covered by bush and mixed forest. Later on, agricultural land dominated the other LC types. For example, cultivated land was nearly threefold by 1984 (Figure 3b, Table 2), showing a near 17% increase in a decade, mainly at the expense of grazing and bushland cover types that exhibited a rapid decrease amounting to nearly 5% and 16%, respectively. In 1995, nearly 77% of the area was covered by bush and agricultural land, of which around 40% of the total was intensively cultivated agriculture. By the year 2003, nearly 42% of the total was covered by agricultural land.

Supervised classification of the 2008 Landsat image (Figure 3e) revealed that the majority of the area was covered by agricultural and bushland cover types accounting for nearly 43 and 46 percent of the total. On the other hand, grazing land and mixed forest covered about 6% of the land area. In 2018, the outcome of image classification showed that about 48% of the watershed was under cultivation (i.e., more than four times the area in 1973) and bushland and grazing land covered nearly 45% and 4% of the total, respectively (Figure 3a, Table 2). There had also been a rapid decline in the grazing and mixed forest LC types between 1973 and 2018. The grazing and mixed forest LC types that covered 13.5% and 16.7% of the area in 1973, respectively, showed a considerable decrease to 4.1% and 2.3%, respectively, in 2018.

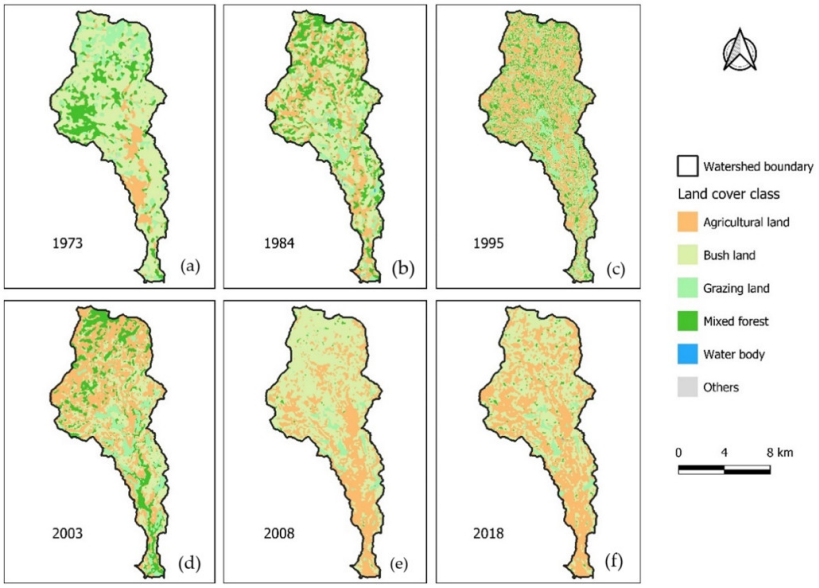

Figure 3. Spatial distribution of LC types in the Batena watershed from 1973 to 2018 (**a**)–(**f**).

Table 2. Change matrix for response of LC (km^2, %) in the Batena watershed.

LC Type	Years											
	1973		1984		1995		2003		2008		2018	
	km^2	%	km^2	%	km^2	%	km^2	%	km^2	%	km^2	%
Agriculture	11.7	10.0	31.0	26.6	46.0	39.5	48.3	41.4	50.2	43.0	56.5	48.4
Bushland	69.7	59.7	51.4	44.2	43.6	37.4	34.9	29.9	54.1	46.4	52.8	45.2
Grazing land	15.8	13.5	10.2	8.8	8.6	7.3	12.2	10.5	5.8	5.0	4.8	4.1
Mixed forest	19.5	16.7	23.9	20.5	18.4	15.8	21.2	18.2	6.6	5.6	2.7	2.3
Total area	116.7		116.7		116.7		116.7		116.7		116.7	
Overall acc.	95.1		99.2		95.2		96.2		98.2		90.4	
$\hat{k}$	92.3		98.4		93.3		97.8		97.1		93.2	

Some other watershed and river basin scale studies conducted in the Ethiopian Rift Valley basin support our finding that agricultural land has increased through time. For example, an LCC study conducted in the central Rift Valley basin (10,320 km^2 area) for a period of 30 years (1985–2015) [63] indicated that there was a rapid increase in irrigable land, large scale farming, and mixed cultivation accounting for 59% of the area. They also noted that over the 30-year period, about 81% of the land showed major changes in LC. Another study [18] conducted in two districts of the Ethiopian central Rift Valley indicated that between 1973 and 2014, there was a significant increase in agricultural areas at the expense of all other LC types. The results reported by [18] showed that between 1973 and 2014, the area of agricultural land increased from 11.0% to 47%, whereas the area of the other three major LC types (i.e., forest, grassland, and woodland) declined by 6%, 13%, and 15%, respectively. A study in the Upper Dijo River watershed, on the midwest escarpment of the Ethiopian Rift Valley [63], that aimed to detect the pattern of LCC for three decades (1972–2004) supports this finding. This study highlighted that shrub and riverine trees declined at rates of 21.5 and 16.3 ha per year, respectively, and agricultural land increased at a rate of 12.5 ha per year.

From the result, it can be inferred that the increasingly noticeable changes in LC in the Batena watershed can alter the fluxes of water, sediment, and other water constituents, which result in significant changes in natural resources and the loss of biodiversity [14]. Consequently, a fine-scale assessment (at watershed level) of the spatiotemporal status of LC and its rate of change is of a paramount importance for developing environmental protection and

sustainability plans [64]. However, though the study has been supported by field validation, LCC assessment at a watershed level is still prone to classification errors. For example, this rural watershed did not have a built-up LC type as the rural settlements were thinly dispersed and sparsely populated. They were classified under the agricultural LC type.

In summary, as indicated in Figure 3, the agricultural areas stretched to a higher altitude. This result is consistent with previous studies conducted to evaluate the impacts of LULC with topography [65]. The extent of different LC types and their rate of change during the study period are summarized in Table 2. In all the study periods, agricultural land showed a progressive increase covering nearly 26.6%, 39.5%, 41.4%, 43%, and 48.4% of the watershed total area in 1984, 1995, 2003, 2008, and 2018, respectively. Compared to the rate of agricultural expansion in the first three decades (i.e., 1973 to 1995), the rate of agricultural expansion in the watershed over the last few years has reduced. This might be due to improved LC management following the greater practice of planting the bush *Ensete ventricosum* (false banana). As a result, during the entire period of analysis, 1973–2018, some conversion of cultivated land to bush and plantation forests was indicated.

There were more active LCCs in the area in the first study period (1973 to 1984) than during the period from 1984 to 1995. In the first decade, nearly half of the landscape underwent LCC and 16.6% of the total that was once bush, forest, and grazing land in 1973 had been converted to agriculture in 1984. Table 2 summarizes the areas of the LC types for six snapshots from 1973 to 2018, with classification accuracy expressed using kappa coefficient ($\hat{k}$).

Land Cover Change Intensity

The intensity of LCC and degree of vegetation restoration is quantified with the VCI (Figure 4). The VCI quantitatively describes the dimension, status, and changes of vegetation in an area over time based on the difference between two LC datasets. As indicated in Figure 4, for example, a 24.4% change in vegetation between 1973 (1) and 2008 (5) was nearly two times the change that occurred between 1984 (2) and 2008. In addition, the vegetation change index between 1973 (1) and 2018 (6) was about five times the change between 1995 (3) and 2018 (6).

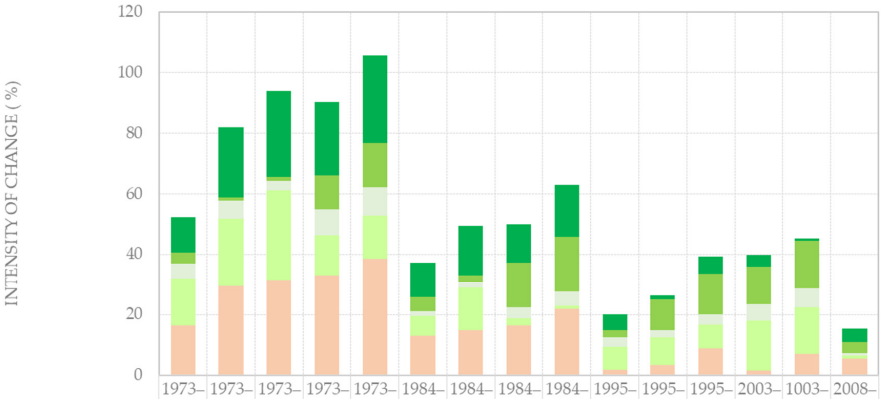

	1973–1984	1973–1995	1973–2003	1973–2008	1973–2018	1984–1995	1984–2003	1984–2008	1984–2018	1995–2003	1995–2008	1995–2018	2003–2008	1003–2018	2008–2018
VCI Vegetation	11.8	23.3	28.3	24.4	28.9	11.4	16.5	12.6	17.1	5.1	1.2	5.7	3.9	0.6	4.5
LCI Mixed forest	3.7	0.9	1.4	11.1	14.5	4.7	2.3	14.8	18.2	2.4	10.1	13.5	12.5	15.9	3.4
LCI Grazing land	4.8	6.2	3.1	8.5	9.4	1.4	1.7	3.8	4.7	3.1	2.4	3.3	5.5	6.4	0.9
LCI Bush land	15.6	22.3	29.8	13.4	14.5	6.7	14.1	2.3	1.1	7.5	9	7.8	16.4	15.3	1.1
LCI Agriculture	16.5	29.4	31.4	33	38.4	12.9	14.9	16.4	21.9	1.9	3.5	8.9	1.6	7	5.4

Figure 4. Absolute value changes: percent vegetation change index (VCI) and LCC intensity index (LCI) for the different land cover types during the different change regimes.

Figure 4 shows the LCI values relating to LCC for each specific LC type, which can also be represented in Figure 4b as the absolute value of change between two LC maps. Regardless of the sign preceding the numbers, a higher numeric value of the LCI for a specific LC type may indicate more intense LCC in the watershed. For example, as indicated

in Figure 4 for agricultural land between 1973 and 2018, the intensity of LCC (38.4%) was nearly twofold of the change between 1973 and 1984. This means that there was an intense change in the agricultural LC type during the specified time. Similarly, between 1973 and 2018, the LCC intensity index for grazing land was 9.4% and dropped to 4.7% between 1984 and 2018.

In summary, change in LC intensity between two specific times is an indication of the change in the magnitude of different LC types, which, in turn, may evidence anthropogenic effects and a regime shift in socioeconomic activities [1]. This can also be evidenced from the change in the magnitude of different LC types between two pairs of LC types as indicated by the LCI values in Figure 4 below.

The change detection statistics shown in Table 3 provide a detailed tabulation of changes between the initial state classes in the rows and the final state classes in the columns. For each initial state class, the table indicates how these LC types were classified in the final state image. To illustrate, between 1973 and 2018, agricultural land (+44.8) showed an increase in the spatial neighborhood at the expense of grazing (−11.0), bush (−16.9), and mixed forest (−16.9) LC types.

Table 3. LC transition matrix (km^2) for the period 1973–2018.

Initial State		Final State (2018)					
		AL	**BL**	**GL**	**MF**	**RT**	**Gain**
1973	AL	8.3	31.4	8.0	8.8	56.5	48.2
	BL	2.6	33.3	6.8	9.9	52.8	19.4
	GL	0.6	3.4	0.6	0.1	4.8	4.1
	MF	0.1	1.5	0.3	0.7	2.7	1.9
	CT	11.7	69.7	15.8	19.5	116.7	
	CC	3.4	36.3	15.1	18.8		
	ID	44.8	−16.9	−11.0	−16.9		
1984	AL	21.0	27.2	4.3	3.9	56.5	35.4
	BL	9.2	22.9	2.0	18.6	52.8	29.9
	GL	0.4	0.4	3.9	0.03	4.8	0.9
	MF	0.3	1.0	0.02	1.4	2.7	1.3
	CT	31.0	51.4	10.2	23.9	116.7	
	CC	9.9	28.5	6.3	22.5		
	ID	25.5	1.3	−5.4	−21.2		
1995	AL	34.2	17.2	3.1	2.0	56.5	22.2
	BL	11.5	24.1	2.1	15.1	52.8	28.7
	GL	0.2	1.1	3.4	0.02	4.8	1.4
	MF	0.1	1.2	0.04	1.3	2.7	1.3
	CT	46.0	43.6	8.6	18.4	116.7	
	CC	11.8	19.6	5.2	17.1		
	ID	10.4	9.1	−3.8	−15.8		
2003	AL	29.7	11.9	5.6	9.3	56.5	26.8
	BL	17.8	21.4	2.5	11.1	52.8	31.4
	GL	0.4	0.2	4.1	0.1	4.8	0.7
	MF	0.45	1.40	0.03	0.77	2.7	1.9
	CT	48.3	34.9	12.2	21.2	116.7	
	CC	18.6	13.6	8.1	20.4		
	ID	8.2	17.8	−7.5	−18.5		
2008	AL	46.0	7.3	0.6	2.6	56.5	10.5
	BL	3.3	43.9	2.4	3.2	52.8	8.9
	GL	0.9	1.6	2.3	0.0	4.8	2.5
	MF		1.3	0.5	0.8	2.7	1.8
	CT	50.2	54.1	5.8	6.6	116.7	
	CC	4.2	10.2	3.5	5.8		
	ID	6.3	−1.3	−1.0	−3.9		

Note: descriptions of the notations are agricultural (AL), bush (BL), grazing land (GL), mixed forest (MF), class total for the specific initial state (CT), class change for the specific initial state (CC), image difference for the specific initial state (ID), and row total (RT).

As indicated in Table 3, the image difference or net change (gain minus loss) was positive for agricultural land for all six reference years at varying degrees and negative for grazing and mixed forest LC types. In line with our findings, Girmay et al. [63] indicated that there was a rapid increase in agricultural land in the central Rift Valley basin where our study area is a contributing subcatchment. Other basin scale studies in the Ethiopian central Rift Valley [18] and midwest escarpment of the Ethiopian Rift Valley [66] have also noted that agricultural land has been increasing through time. According to Mengistu et al. [66], for example, between 1972 and 2004, agricultural land increased at a rate of 12.5 hectare per year.

3.2. Relationship of Soil, Topography, and Land Cover

3.2.1. Soil Spatial Analysis, Classification, and Mapping

Table S1 shows the ranking of qualifiers [53] based on the FAO reference soil group guidelines [67]. Following the field soil survey, laboratory analysis, and descriptive augers, seven soil taxa at the family level of the USDA soil taxonomy hierarchy were identified and mapped. These soil types were chromic luvisol, chromic vertisol, haplic gleysol, humic nitisol, lithic leptosol, ochric regosol, and pellic vertisol. Approximately 92% of the study area was covered with three soil types: pellic vertisol (28.2%), chromic luvisol (30.2%), and chromic vertisol (33.3%). The remaining soil classes (humic nitisol, haplic gleysol, lithic leptosol, and ochric regosol) covered 8% of the area.

The relationship between soil, LC distribution, and terrain slope in the watershed is illustrated in Figure 5. Agricultural lands were mostly located in regions of lower altitude. The continuous conversion of different LC types into agricultural land had squeezed bush and forest covers for all slope ranges from low (slope class 1) to very steep (slope class 5) terrains. The conversion of LC was location dependent. To illustrate, on the upper terrain slope of the watershed a slight change in LC was observed as opposed to the major change on the lower slopes. Following the growing practice of planting the bush *Ensete ventricosum* (false banana), there was a more variable trend in the bush LC type. Soil–LC–slope relationships and the spatial variability in LC types can be collated based on six snapshots (1973–2018) for five slope classes. For example, in 1973 (Figures 5 and 6), 25 ha of the agricultural area was topographically located in slope class 1 (slope ranging from 0 to 2°) and the specific soil type was chromic vertisol (VRx).

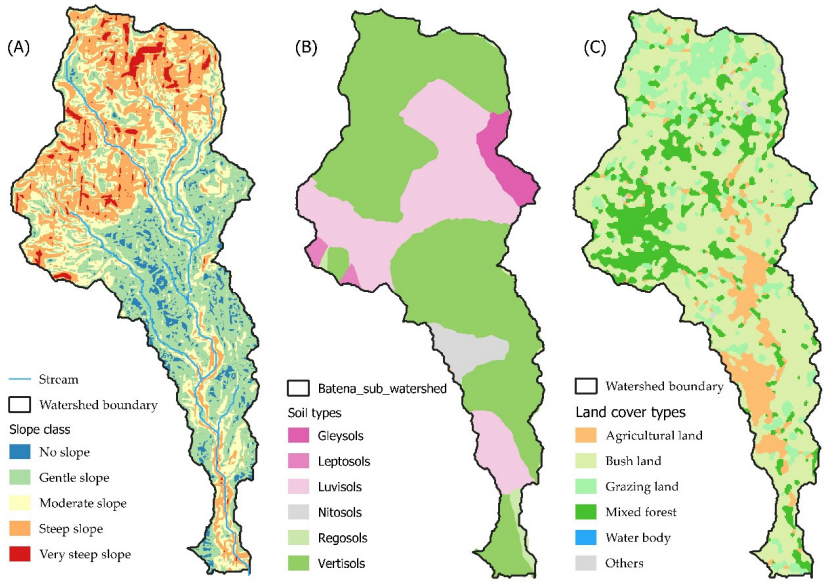

Figure 5. Relationship of slope classes (**A**), soil types (**B**), and land cover classes (**C**) in Batena watershed. The land cover map (**C**) is for 1993 and is shown here to illustrate the pattern of land cover types at the start.

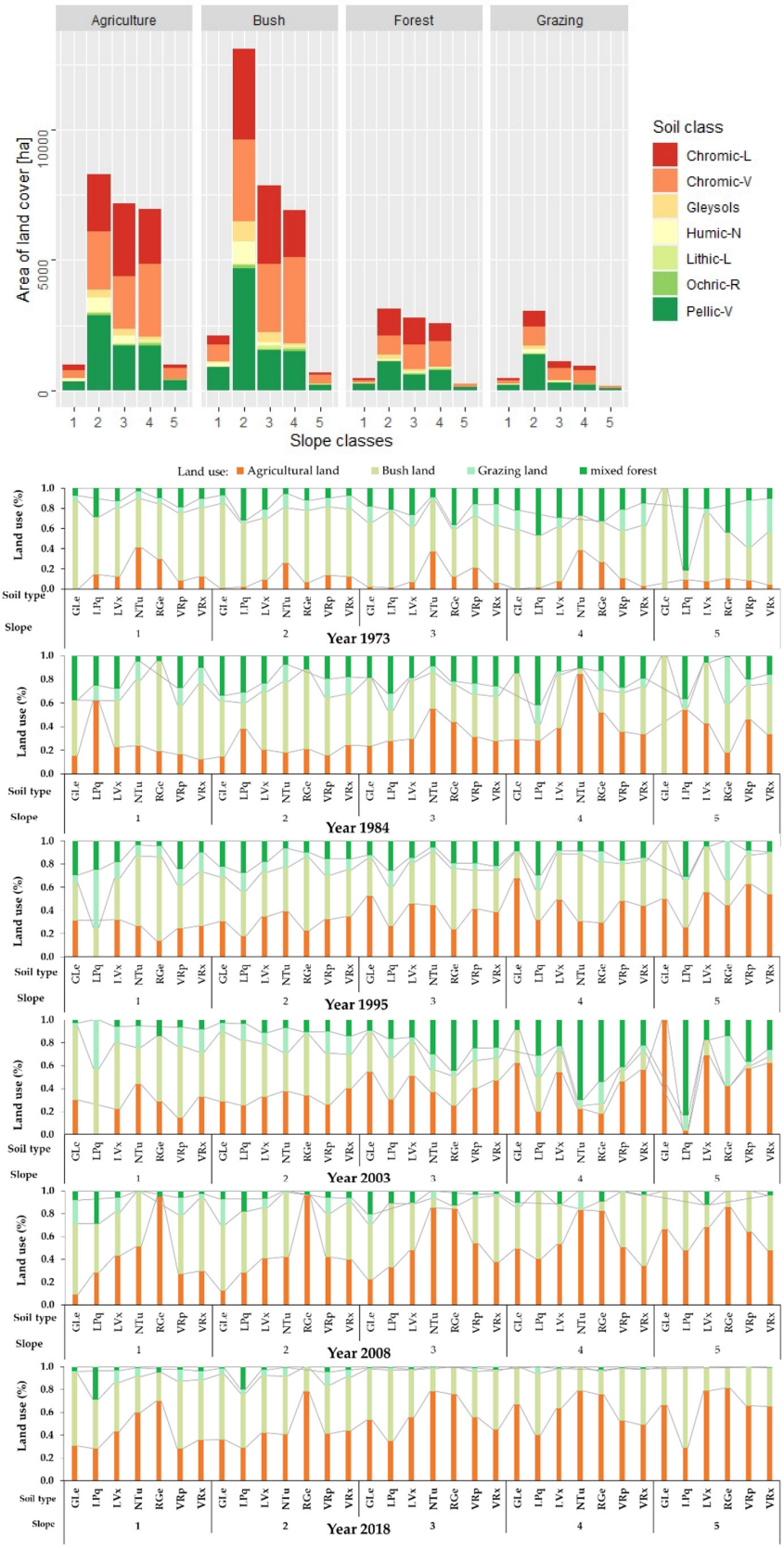

Figure 6. Area of each LC type (in ha) by slope classes and soil types in the Batena watershed. The detailed description of the acronyms of soil types is presented in Figure 5. Slope classes denoted by 1, 2, 3, 4, and 5 represent slope in degrees in the ranges: 0–2, 2–10, 10–15, 15–30, and >30, respectively.

As an important indicator of topography, terrain slope has a substantial effect on LCC, thereby affecting soil fertility, and LC density and pattern. LC changed dramatically in agriculturally accessible and arable soils (Figure 6) and remained relatively stable in mountainous and poorly fertile soils [68]. The intensification of agricultural practices could also be related to the acute shortage of land on the gentle slopes. Changes in LC are usually accompanied by a decrease in the concentrations of soil organic carbon and nutrients and also a deterioration in soil structure. Similar studies in other geographic locations [69,70] have highlighted that in line with agricultural unsuitability, properties of dryness/wetness and magnitude and the seasonal pattern of rainfall are the other possible variables to alter the pattern and trend of LCC. This suggests that the management of any one of these soil properties may yield unintended cascading effects throughout the soil subsystem.

According to the FAO [47], soils such as vertisols (VRx, VRp), luvisols (LVx), nitisols (NTu), and gleysols (GLe) are fertile and highly suitable for agriculture. On the other hand, leptosols (LPq) and regosols (RGe) are very weakly developed mineral soils in unconsolidated materials that are extensive in eroding lands, in particular in arid and semi-arid areas and mountain regions.

Figure 6 indicates that most of the land cover classes and soil types occur in the second, third, and fourth slope classes, respectively. Agriculture and bushland accounted for the majority of the land areas in the study area in general and in the middle slope classes described above in particular (Table 2 and Figure 6). The proportion of agricultural land cover increased in recent years (Figure 6 bottom panel) but that of bushland sustained a significantly large share from the start. The increase in agricultural land cover happened at the expense of the loss of forest and grazing lands. Pelvic vertisols, chromic vertisols, and chromic leptosols dominate these slope classes. The size of land with extremely low and high slope classes was small. However, even these small patches of land were used for agriculture.

3.2.2. Terrain Effects on Soil Physicochemical Properties and Land Cover Distribution

As an important indicator of topography, slope gradient has a clear effect on the intensity of soil erosion [71], thereby affecting soil fertility and patterns of LC (Figurs 3 and 7). Steeper slopes generally have rapid runoff, less moisture entering the soil [72], and lower crop productivity. Regarding the effect of slope under the different land cover status at any point in the landscape, Tables S2 and S3 and Figure 7 illustrate the spatial relation between slope and selected soil physicochemical properties, such as sand, clay, silt, available water content (AWC), and soil organic carbon contents (OC). Considering the spatial variation in soil's AWC can help to define the amount of water stored in the root zone and determine the length of time that a plant can survive between rain events. In order to evaluate the impact of slope on soil texture (sand, clay, and silt), the OC and AWC, and the spatial variation in each variable is presented in Figure 7. Changes in the OC and AWC are highly related to variations in soil type and LC (Tables S2 and S3). For example, a highly leached leptosol has low OC.

Other similar studies conducted in the north central highlands of Ethiopia [73] indicate that the variation in these soil physicochemical properties is highly related to topographic position and LC. According to their findings, for example, the lowest soil pH was observed in the upper slope positions, which are forested areas characterized by high OC, while the highest pH value was recorded on lower slope positions with low OC where cultivation land was the dominant LC. Griffiths et al. [74] showed a clear association between topographical parameters such as slope, surface curvature, elevation, and LC and OC variation. They reported that topography could influence soil physicochemical properties (OC, soil depth, texture, and mineral contents), thereby affecting grain and biomass production. Supporting our finding of the LC–soil property–slope relationships, Hu et al. [75] reported a decrease in the OC and associated changes in the local microenvironment and soil nutrients with LC conversions into agriculture and an increasing incidence of tillage. Scientific evidences from different areas revealed similar patterns of soil property change.

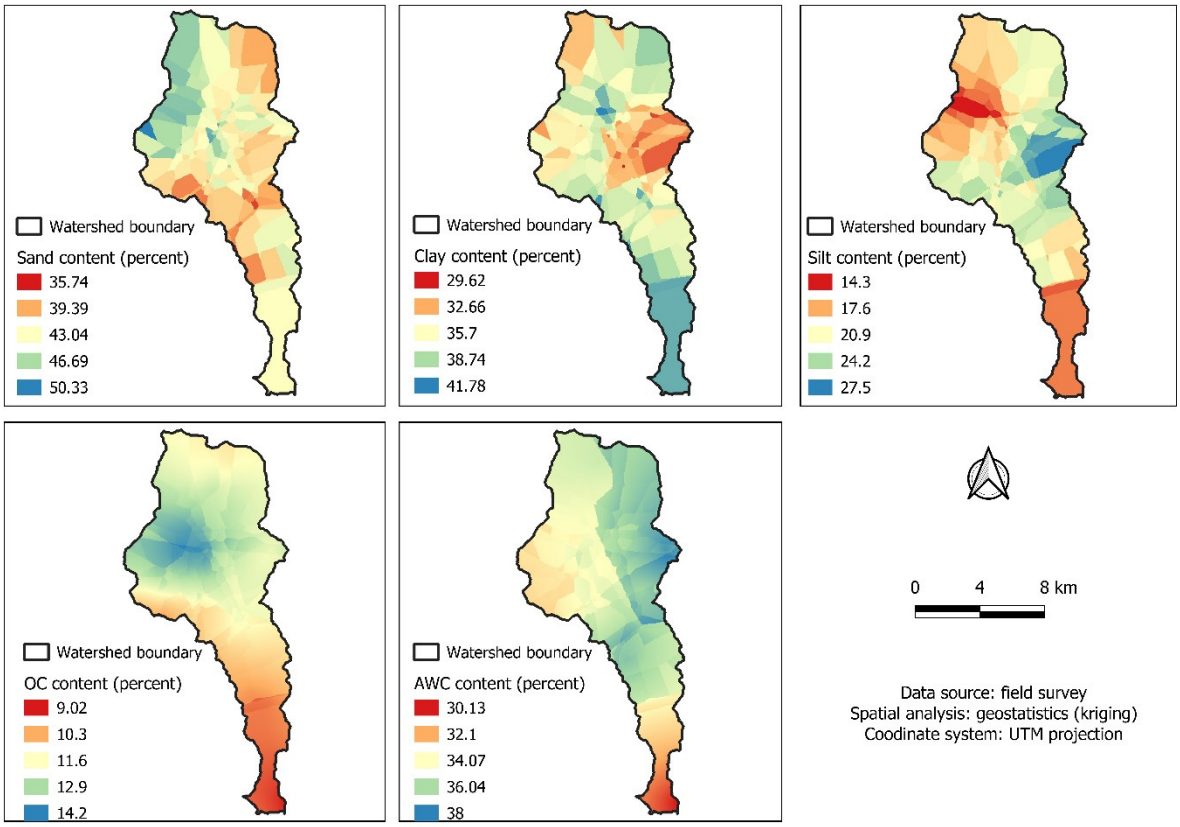

Figure 7. Classification of soil properties. Note that OC and AWC represent organic carbon and available water content, respectively.

Further details of terrain effects on soil physicochemical properties and LC distribution can be found in Tables S2 and S3. The descriptive statistics of soil physical attributes with altitude are also presented in depth in the Supplementary Materials (see Tables S1–S5 and Figure S1). The spatial distribution of LC was significantly affected by soil type and fertility, and slope position. For example, in 2018, 19.8 ha of the agricultural area was located in slope class 2 (slope ranging from 2 to 10°) in a silty soil type 3 (i.e., abundance between 22.7–27.5%). From field sampling and laboratory analysis results, we also presented the spatial correlation between soil's physical and chemical properties using Pearson, Spearman's rho, and Kendall's rank correlation coefficient for top and second soil layers (Tables S4 and S5). Figure 7 illustrates the spatial relation of the selected soils' physical and chemical properties.

3.3. Socioeconomic Impacts of Land Cover Change

Through time, rapid population growth has been accompanied by the considerable expansion in agricultural land, which has been noticeable in Ethiopia since the late half of the 20th century [14]. According to Ariti et al. [18], the Central Rift Valley basin is typified with agricultural expansion at the expense of all other LC types. In their findings, it was indicated that between 1973 and 2014, the rate and magnitude of LCC for four major LC types; water, forest, grass, and woodland declined by 3, 6, 13, and 15%, respectively, as a result of a 36% increase in agricultural area. This dynamic change in LC has resulted in significant socioeconomic pressures in the Ethiopian Rift Valley, which is home to many unique aquatic and terrestrial ecosystems with documented evidence of natural resources' degradation [14]. The degradation of natural resources and loss of biodiversity are therefore the most visible socioeconomic and environmental problems in the Rift Valley lakes basin, and put increasing pressures on many water bodies.

Several other studies [14,76–79] have reported that LCC has considerable socioeconomic impacts. For example, a study conducted in the Rib watershed that forms part of the northwestern highlands of the Blue Nile basin of Ethiopia indicated multiple effects of LCC in the area [22]. The authors [22] explained that LCC has significantly affected the ecological and socioeconomic conditions of the watershed as it has been identified as one of the most important causes of soil quality deterioration. Other studies conducted to identify determinants of farmers' adoption of land management practices in the northern highlands of Ethiopia indicated that LCC accelerates the loss of topsoil and aggravates erosion [78].

Soil erosion resulting from changes in LC affects the environment in various ways [80,81]. For example, the conversion of LC types from either forest or bushland to agriculture loosens the surface protection, provoking splash erosion and soil erodibility, especially in steeper areas of the watershed [82], thereby increasing the loss of soil nutrients. The soil eroded from upstream of the watershed is then routed downstream and accumulates in the lower reaches through sedimentation. In addition to inadequate watershed management practices, extensive agriculture in the upstream areas results in high runoff and sediment accumulation in the downslope areas and river banks [83]. This is particularly critical in the study area, a tributary of the Rift Valley lakes basin that drains to the Bilate river, which later empties into Lake Abaya. For example, a basin scale LC assessment [63] in the central Rift Valley showed that 81% of the land indicated major changes in LC, and the lake area decreased by 2.31%. According to their findings, one of the Rift Valley lakes, Lake Abijata, showed a progressive decline of 25.6%.

For the six LCC periods considered in this study (see Section 3.1), there has been a significant change from bush and forest to agricultural LC. This change in LC from vegetation into agriculture and the corresponding land disturbance accelerates soil erosion, thereby bringing a reduction in soil infertility in the area. As detailed in the data and methods supplemented by comprehensive results, and our analysis of the soil–topography and LUC interactions, the findings of the research provide immense contributions to the science in the field as they explain how agricultural land use has changed over the decades at different topographies and soil types. Our findings basically show that agricultural use expanded around fertile soils and the most suitable topography. This analysis is essential to control land degradation, to prioritize areas for watershed management, and mitigate the effects of future climate extreme events. Zenebe et al. [84] highlighted that relating land use change with terrain dynamics could provide a platform to inform policy makers towards land management decisions. Given such implications for basin-wide water sustainability, we thereby suggest a continued undertaking of a long-term LULC study in regional endorheic basins.

4. Conclusions

Over the last few decades, more than 90% of Ethiopian highlands have undergone dramatic LCCs that have ultimately affected the country's socioeconomic and environmental situation. As with other parts of the country's highlands, the study area in the Great Rift Valley basin has undergone major changes in LC. In areas with heterogeneous topography and where soil is spatially variable, the way we manage catchment LC alters the fluxes of water, sediment, and nutrient balance. This effect is more pronounced in highly rugged agrarian landscapes where there is a significant land disturbance and topographic influences are dominant. Having a knowledge of soil properties and terrain attributes associated with the prevailing anthropogenic LCC is vital for ensuring sustainable land management. However, previous studies on the spatial variability in LC and soil properties have either been site-specific, coarse in scale, or implemented pedo-transfer-functions (PTFs) that neither accounted for environmental effects nor provided all the required data inputs.

In this study, we assessed spatiotemporal land cover change and soil–landscape relationships and mapped soil property spatial dynamics to understand landscape physicochemical processes. The significance of this study therefore stems from the method and

the findings achieved to parametrize scale effects. We explained the drawbacks of relying on either coarse resolution data that assign the same attribute values for areas at different gradients or site-specific and unreliable PTFs. We ascertained spatiotemporal variations in landscape datasets through a rigorous field survey and laboratory analysis and developed soil–LC relations for a tropical catchment in the Rift Valley basin where data are scarce. Descriptive statistics were used to explore soil–terrain dynamics and to associate soil–land use–terrain interactions.

The time series LCC (between the years: 1973, 1984, 1995, 2003, 2008, and 2018) indicated that the area experienced an increase in agricultural land at the expense of other LC types such as bushland, grazing land, and mixed forest, which attests to the ongoing deforestation and drought. For example, agricultural land that covered 10% of the watershed in 1973 had increased by nearly fivefold by 2018, accounting for 48.4% of the area of the watershed. The study also characterized the soil–LC–topography interaction in which we explored the effects of terrain characteristics on soil's physicochemical properties and the LC distribution in the area. The study results revealed that the spatial variability in LCC was significantly affected by soil type and slope. We advise that similar studies should be conducted in different environmental settings to check if similar patterns exist.

Supplementary Materials: The following supporting information can be downloaded at: https://www.mdpi.com/article/10.3390/rs14143257/s1, see Table S1: soil classification; Tables S2 and S3: soil–LU–slope interaction; Table S4: first soil layer; Table S5: second soil layer in the supplementary excel file. A note for the value range of each of the soil physicochemical properties, slope range (°), and time series LCC is included. Figure S1: catchment characteristics and selected soil physicochemical properties. Catchment characteristics: slope and sampling sites, soils, and selected soil physicochemical properties: sand (%), clay (%), silt (%), OM (%), EC (S/m), AWC, Ksat, MBD, Aspect, and TI.

Author Contributions: Conceptualization, G.T.A., H.T. and A.M.S.; research idea and field sampling protocol, G.T.A.; methodology, G.T.A., H.T., A.M.S., M.A.J. and A.M.M.; resources, G.T.A. and A.M.M.; supervision, H.T., S.S.D., C.E.N., D.P.H., A.M.M., J.L.A. and J.J.; writing—original draft, G.T.A.; funding acquisition, G.T.A. and S.S.D.; writing—review and editing, all authors. A.M.S. contributed equally to this paper. All authors have read and agreed to the published version of the manuscript.

Funding: This research was funded by the International Water Management Institute (IWMI) grant number SAP PO45—12069 through the Nile Basin Development Challenge of the CGIAR challenge program for Water and food and Bahir Dar University—Blue Nile Water Institute (grant number: 1/26971/1.11.10).

Acknowledgments: Gebiaw T. Ayele would like to acknowledge for assisting the research under the project "Remote sensing approaches to access drought severity from multi-temporal GIMMS NDVI, rainfall and PDSI interactions for future drought monitoring". We thank Graeme Curwen of the Australian Rivers Institute for his support with additional technical details and suggestions.

Conflicts of Interest: The authors declare no conflict of interest.

References

1. Pitman, A.; de Noblet-Ducoudré, N. *Human Effects on Climate through Land-Use Induced Land Cover Change*; Future of the World's Climate/Elsevier: Amsterdam, The Netherlands, 2011; pp. 77–95. [CrossRef]
2. Oliver, T.H.; Morecroft, M.D. Interactions between climate change and land use change on biodiversity: Attribution problems, risks, and opportunities. *Wiley Interdiscip. Rev. Clim. Chang.* **2014**, *5*, 317–335. [CrossRef]
3. Ayele, G.T.; Tebeje, A.K.; Demissie, S.S.; Belete, M.A.; Jemberrie, M.A.; Teshome, W.M.; Mengistu, D.T.; Teshale, E.Z. Time series land cover mapping and change detection analysis using geographic information system and remote sensing, Northern Ethiopia. *Air Soil Water Res.* **2018**, *11*. [CrossRef]
4. Sahana, M.; Hong, H.Y.; Sajjad, H. Analyzing urban spatial patterns and trend of urban growth using urban sprawl matrix: A study on Kolkata urban agglomeration, India. *Sci. Total Environ.* **2018**, *629*, 1557–1566. [CrossRef]
5. Houet, T.; Loveland, T.R.; Hubert-Moy, L.; Gaucherel, C.; Napton, D.; Barnes, C.A.; Sayler, K. Exploring subtle land use and land cover changes: A framework for future landscape studies. *Landsc. Ecol.* **2010**, *25*, 249–266. [CrossRef]

6. Rechkemmer, A.; von Falkenhayn, L. The human Dimensions of Global Environmental Change: Ecosystem Services, Resilience, and Governance. Erca: From the Human Dimensions of Global Environmental Change to the Observation of the Earth from Space. *EPJ Web Conf.* **2009**, *8*, 3–17. [CrossRef]
7. Ayele, G.T.; Teshale, E.Z.; Yu, B.F.; Rutherfurd, I.D.; Jeong, J. Streamflow and sediment yield prediction for watershed prioritization in the upper blue nile river basin, ethiopia. *Water* **2017**, *9*, 782. [CrossRef]
8. Getachew, H.E.; Melesse, A.M. The impact of land use change on the hydrology of the Angereb watershed, Ethiopia. *Int. J. Water Sci.* **2012**, *1*. [CrossRef]
9. Mango, L.M.; Melesse, A.M.; Mc Clain, M.E.; Gann, D.; Setegn, S.G. Land use and climate change impacts on the hydrology of the upper Mara River Basin, Kenya: Results of a modeling study to support better resource management. *Hydrol. Earth Syst. Sci.* **2011**, *15*, 2245–2258. [CrossRef]
10. Mango, L.M.; Melesse, A.M.; McClain, M.E.; Gann, D.; Setegn, S.G. Hydro-meteorology and water budget of the Mara River Basin under land use change scenarios. In *Nile River Basin*; Springer: Dordrecht, The Netherlands, 2011; pp. 39–68.
11. Mohammed, H.; Alamirew, A.; Assen, M.; Melesse, A. *Spatiotemporal Mapping of Land Cover in Lake Hardibo Drainage Basin, Northeast Ethiopia: 1957–Water Conservation: Practices, Challenges and Future Implications*; Nova Publishers: New York, NY, USA, 2013.
12. Wondie, M.; Schneider, W.; Melesse, A.M.; Teketay, D. Spatial and temporal land cover changes in the simen mountains national park, a world heritage site in northwestern ethiopia. *Remote Sens.* **2011**, *3*, 752–766. [CrossRef]
13. Hurni, H.; Abate, S.; Bantider, A.; Debele, B.; Ludi, E.; Portner, B.; Yitaferu, B.; Zeleke, G. Land Degradation and Sustainable Land Management in the Highlands of Ethiopia. 2010, pp. 187–207. Available online: https://boris.unibe.ch/5959/1/Hurni_Land%20degradation.pdf (accessed on 4 May 2022).
14. Elias, E.; Seifu, W.; Tesfaye, B.; Girmay, W. Impact of land use/cover changes on lake ecosystem of Ethiopia central rift valley. *Cogent Food Agric.* **2019**, *5*, 1595876. [CrossRef]
15. Verburg, P.H.; Crossman, N.; Ellis, E.C.; Heinimann, A.; Hostert, P.; Mertz, O.; Nagendra, H.; Sikor, T.; Erb, K.H.; Golubiewski, N.; et al. Land system science and sustainable development of the earth system: A global land project perspective. *Anthropocene* **2015**, *12*, 29–41. [CrossRef]
16. Gebreslassie, H. Land use-land cover dynamics of Huluka watershed, Central Rift Valley, Ethiopia. *Int. Soil Water Conserv. Res.* **2014**, *2*, 25–33. [CrossRef]
17. Mengistu, K.T. Watershed Hydrological Responses to Changes in Land Use and Land Cover, and Management Practices at Hare Watershed, Ethiopia. Ph.D. Thesis, der Universität Siegen, Sigen, Germany, 2009.
18. Ariti, A.T.; van Vliet, J.; Verburg, P.H. Land-use and land-cover changes in the Central Rift Valley of Ethiopia: Assessment of perception and adaptation of stakeholders. *Appl. Geogr.* **2015**, *65*, 28–37. [CrossRef]
19. Asres, R.S.; Tilahun, S.A.; Ayele, G.T.; Melesse, A.M. Analyses of Land Use/Land Cover Change Dynamics in the Upland Watersheds of Upper Blue Nile Basin. In *Landscape Dynamics, Soils and Hydrological Processes in Varied Climates*; Springer: Cham, Switzerland, 2016; pp. 73–91.
20. Betru, T.; Tolera, M.; Sahle, K.; Kassa, H. Trends and drivers of land use/land cover change in Western Ethiopia. *Appl. Geogr.* **2019**, *104*, 83–93. [CrossRef]
21. Etefa, G.; Frankl, A.; Lanckriet, S.; Biadgilgn, D.; Gebreyohannes, Z.; Amanuel, Z.; Poesen, J.; Nyssen, J. Changes in land use/cover mapped over 80 years in the Highlands of Northern Ethiopia. *J. Geogr. Sci.* **2018**, *28*, 1538–1563. [CrossRef]
22. Moges, D.M.; Bhat, H.G. An insight into land use and land cover changes and their impacts in Rib watershed, north-western highland Ethiopia. *Land Degrad. Dev.* **2018**, *29*, 3317–3330. [CrossRef]
23. Dodgson, N.A. *Image Resampling*; University of Cambridge, Computer Laboratory: Cambridge, UK, 1992.
24. Ceddia, M.B.; Vieira, S.R.; Villela, A.L.O.; Mota, L.D.S.; Anjos, L.H.C.D.; Carvalho, D.F.D. Topography and spatial variability of soil physical properties. *Sci. Agric.* **2009**, *66*, 338–352. [CrossRef]
25. O'Geen, A. Soil water dynamics. *Nat. Educ. Knowl.* **2012**, *3*, 12.
26. Luo, Y.; Yang, S.; Zhao, C.; Liu, X.; Liu, C.; Wu, L.; Zhao, H.; Zhang, Y. The effect of environmental factors on spatial variability in land use change in the high-sediment region of China's Loess Plateau. *J. Geogr. Sci.* **2014**, *24*, 802–814. [CrossRef]
27. Rawat, J.S.; Kumar, M. Monitoring land use/cover change using remote sensing and GIS techniques: A case study of Hawalbagh block, district Almora, Uttarakhand, India. *Egypt. J. Remote Sens. Space Sci.* **2015**, *18*, 77–84. [CrossRef]
28. Otukei, J.R.; Blaschke, T. Land cover change assessment using decision trees, support vector machines and maximum likelihood classification algorithms. *Int. J. Appl. Earth Obs. Geoinf.* **2010**, *12*, S27–S31. [CrossRef]
29. Li, G.; Lu, D.; Moran, E.; Sant'Anna, S.J. Comparative analysis of classification algorithms and multiple sensor data for land use/land cover classification in the Brazilian Amazon. *J. Appl. Remote Sens.* **2012**, *6*, 061706. [CrossRef]
30. Blaschke, T. Object based image analysis for remote sensing. *ISPRS J. Photogramm. Remote Sens.* **2010**, *65*, 2–16. [CrossRef]
31. Suleiman, Y.; Saidu, S.; Abdulrazaq, S.; Hassan, A.; Abubakar, A. The dynamics of land use land cover change: Using geospatial techniques to promote sustainable urban development in Ilorin Metropolis, Nigeria. *Asian Rev. Environ. Earth Sci.* **2014**, *1*, 8–15.
32. Xu, W.X.; Gu, S.; Zhao, X.Q.; Xiao, J.S.; Tang, Y.H.; Fang, J.Y.; Zhang, J.; Jiang, S. High positive correlation between soil temperature and NDVI from 1982 to 2006 in alpine meadow of the Three-River Source Region on the Qinghai-Tibetan Plateau. *Int. J. Appl. Earth Obs. Geoinf.* **2011**, *13*, 528–535. [CrossRef]
33. Sexton, J.O.; Urban, D.L.; Donohue, M.J.; Song, C.H. Long-term land cover dynamics by multi-temporal classification across the Landsat-5 record. *Remote Sens. Environ.* **2013**, *128*, 246–258. [CrossRef]

34. Ahmad, A.; Quegan, S. Analysis of Maximum Likelihood Classification Technique on Landsat 5 TM Satellite Data of Tropical Land Covers. In Proceedings of the 2012 IEEE International Conference on Control, System, Computing and Engineering (ICCSCE 2012), Penang, Malaysia, 23–25 November 2012; pp. 280–285.
35. Li, M.; Zang, S.Y.; Zhang, B.; Li, S.S.; Wu, C.S. A Review of Remote Sensing Image Classification Techniques: The Role of Spatio-contextual Information. *Eur. J. Remote Sens.* **2014**, *47*, 389–411. [CrossRef]
36. Singh, A. Review article digital change detection techniques using remotely-sensed data. *Int. J. Remote Sens.* **1989**, *10*, 989–1003. [CrossRef]
37. Benito-Calvo, A.; De la Torre, I.; Mora, R.; Tibebu, D.; Morán, N.; Martínez-Moreno, J. *Geoarchaeological Potential of the Western Bank of the Bilate River (Ethiopia)*; Analele Universitatii din Oradea XVIISeria Geographie: Madrid, Spain, 2007; pp. 99–104.
38. Roy, D.P.; Ju, J.C.; Kline, K.; Scaramuzza, P.L.; Kovalskyy, V.; Hansen, M.; Loveland, T.R.; Vermote, E.; Zhang, C.S. Web-enabled Landsat Data (WELD): Landsat ETM plus composited mosaics of the conterminous United States. *Remote Sens. Environ.* **2010**, *114*, 35–49. [CrossRef]
39. Crippen, R.E. A simple spatial filtering routine for the cosmetic removal of scan-line noise from Landsat TM P-tape imagery. *Photogramm. Eng. Remote Sens.* **1989**, *55*, 327–331.
40. Richards John, A.; Xiuping, J. *Remote Sensing Digital Image Analysis: An Introduction*; Springer: Berlin, Germany, 1999.
41. Ju, J.C.; Roy, D.P.; Vermote, E.; Masek, J.; Kovalskyy, V. Continental-scale validation of MODIS-based and LEDAPS Landsat ETM plus atmospheric correction methods. *Remote Sens. Environ.* **2012**, *122*, 175–184. [CrossRef]
42. Bakker, W.H.; Grabmaier, K.; Hunmeman, G.; Van Der Meer, F.; Prakash, A.; Tempfli, K.; Gieske, A.; Hecker, C.; Janseen, L.; Parodi, G. *Principles of Remote Sensing, An Introductory Textbook*; The International Institute for Geo-Informational Science and Earth Observation (ITC): Enschede, The Netherlands, 2004.
43. Serra, P.; Pons, X.; Sauri, D. Post-classification change detection with data from different sensors: Some accuracy considerations. *Int. J. Remote Sens.* **2003**, *24*, 4975–4976. [CrossRef]
44. Sabins, F.F., Jr.; Ellis, J.M. *Remote Sensing: Principles, Interpretation, and Applications*; Waveland Press: Long Grove, IL, USA, 2020.
45. Mesfin, D.; Simane, B.; Belay, A.; Recha, J.W.; Taddese, H. Woodland cover change in the Central Rift Valley of Ethiopia. *Forests* **2020**, *11*, 916. [CrossRef]
46. Lu, D.; Mausel, P.; Batistella, M.; Moran, E. Land-cover binary change detection methods for use in the moist tropical region of the Amazon: A comparative study. *Int. J. Remote Sens.* **2005**, *26*, 101–114. [CrossRef]
47. World Reference Base for Soil Resources. *A Framework for International Classification, Correlation and Communication*; World Soil Resources Reports; Resources: Rome, Italy, 2006; Volume 103.
48. Sachez-Reyes, U.J.; Nino-Maldonado, S.; Barrientos-Lozano, L.; Trevino-Carreon, J. Assessment of Land Use-Cover Changes and Successional Stages of Vegetation in the Natural Protected Area Altas Cumbres, Northeastern Mexico, Using Landsat Satellite Imagery. *Remote Sens.* **2017**, *9*, 712. [CrossRef]
49. Mas, J.-F. Monitoring land-cover changes: A comparison of change detection techniques. *Int. J. Remote Sens.* **1999**, *20*, 139–152. [CrossRef]
50. Congalton, R.G.; Green, K. *Assessing the Accuracy of Remotely Sensed Data: Principles and Practices*; CRC Press: Boca Raton, FL, USA, 2002.
51. Anderson, J.R. *A Land Use and Land Cover Classification System for Use with Remote Sensor Data*; US Government Printing Office: Washington, WA, USA, 1976; Volume 964.
52. Congalton, R.G. Accuracy assessment: A critical component of land cover mapping. *Gap Anal.* **1996**. [CrossRef]
53. United States Department of Agriculture, Soil Taxonomy. *A Basic System of Soil Classification for Making and Interpreting Soil Surveys*; USDA: Pittsburgh, PA, USA, 1999; Volume 436, pp. 96–105.
54. Webster, R. Is soil variation random? *Geoderma* **2000**, *97*, 149–163. [CrossRef]
55. Isaaks, E.; Srivastava, R. *Applied Geostatistics. An Introduction to Applied Geoestatistics*; Oxford University Press: Oxford, UK, 1989.
56. Ayele, G.T.; Demissie, S.S.; Jemberrie, M.A.; Jeong, J.; Hamilton, D.P. Terrain Effects on the Spatial Variability of Soil Physical and Chemical Properties. *Soil Syst.* **2019**, *4*, 1. [CrossRef]
57. Morgan, C.J. Theoretical and Practical Aspects of Variography: In Particular, Estimation and Modelling of Semi-Variograms over Areas of Limited and Clustered or Widely Spaced Data in a Two-Dimensional South African Gold Mining Context. Ph.D. Thesis, University of the Witwatersrand, Johannesburg, South Africa, 2011.
58. Mcbratney, A.B.; Webster, R. Choosing Functions for Semi-Variograms of Soil Properties and Fitting Them to Sampling Estimates. *J. Soil Sci.* **1986**, *37*, 617–639. [CrossRef]
59. Warrick, A. Spatial variability of soil physical properties in the field. *Appl. Soil Phys.* **1980**, 319–344. Available online: https://www.researchgate.net/publication/300071023_Spatial_Variability_of_Soil_Physical_Properties_in_a_Cultivated_Field (accessed on 4 May 2022).
60. Assefa, F.; Elias, E.; Soromessa, T.; Ayele, G.T. Effect of changes in land-use management practices on soil physicochemical properties in Kabe Watershed, Ethiopia. *Air Soil Water Res.* **2020**, *13*. [CrossRef]
61. Kumar, A.; Padbhushan, R.; Singh, Y.K.; Kohli, A.; Ghosh, M. Soil organic carbon under various land uses in alfisols of Eastern India. *Indian J. Agril. Sci.* **2021**, *91*, 975–979.
62. Coburn, T.C. *Geostatistics for Natural Resources Evaluation*; Taylor & Francis: Milton Park, UK, 2000.
63. Girmay, W.; Tesfaye, B.; Seifu, W.; Elias, E. Effect of Land Use/Cover Changes on Ecological Landscapes of the Four Lakes of Central Rift Valley Ethiopia. *J. Environ. Earth Sci.* **2017**, *7*, 12.

64. Muzein, B.S. Remote Sensing & GIS for Land Cover, Land Use Change Detection and Analysis in the Semi-Natural Ecosystems and Agriculture Landscapes of the Central Ethiopian Rift Valley. 2006. Available online: http://www.vinr.ir/sites/default/files/Muzein2006.pdf (accessed on 4 May 2022).
65. How Jin Aik, D.; Ismail, M.H.; Muharam, F.M.; Alias, M.A. Evaluating the impacts of land use/land cover changes across topography against land surface temperature in Cameron Highlands. *PLoS ONE* **2021**, *16*, e0252111. [CrossRef] [PubMed]
66. Mengistu, D.K.; Woldetsadik, M. Detection and analysis of land-use and land-cover changes in the Midwest escarpment of the Ethiopian Rift Valley. *J. Land Use Sci.* **2012**, *7*, 239–260. [CrossRef]
67. Spaargaren, O.C.; Deckers, J. The world reference base for soil resources. In *Soils of Tropical Forest Ecosystems*; Springer: Berlin, Germany, 1998; pp. 21–28.
68. de Valenca, A.W.; Vanek, S.J.; Meza, K.; Ccanto, R.; Olivera, E.; Scurrah, M.; Lantinga, E.A.; Fonte, S.J. Land use as a driver of soil fertility and biodiversity across an agricultural landscape in the Central Peruvian Andes. *Ecol. Appl.* **2017**, *27*, 1138–1154. [CrossRef]
69. Jemberie, M.A.; Awass, A.A.; Melesse, A.M.; Ayele, G.T.; Demissie, S.S. Seasonal Rainfall-Runoff Variability Analysis, Lake Tana Sub-Basin, Upper Blue Nile Basin, Ethiopia. In *Landscape Dynamics, Soils and Hydrological Processes in Varied Climates*; Springer: Cham, Switzerland, 2016. [CrossRef]
70. Seka, A.M.; Awass, A.A.; Melesse, A.M.; Ayele, G.T.; Demissie, S.S. Evaluation of the Effects of Water Harvesting on Downstream Water Availability Using SWAT. In *Landscape Dynamics, Soils and Hydrological Processes in Varied Climates*; Springer: Cham, Switzerland, 2016. [CrossRef]
71. Conforti, M.; Buttafuoco, G. Assessing space–time variations of denudation processes and related soil loss from 1955 to 2016 in southern Italy (*Calabria region*). *Environ. Earth Sci.* **2017**, *76*, 457. [CrossRef]
72. Balba, A.M. *Management of Problem Soils in Arid Ecosystems*; CRC Press: Boca Raton, FL, USA, 2018.
73. Abate, N.; Kibret, K. Effects of land use, soil depth and topography on soil physicochemical properties along the toposequence at the Wadla Delanta Massif, Northcentral Highlands of Ethiopia. *Environ. Pollut* **2016**, *5*, 57–71. [CrossRef]
74. Griffiths, R.P.; Madritch, M.D.; Swanson, A.K. The effects of topography on forest soil characteristics in the Oregon Cascade Mountains (USA): Implications for the effects of climate change on soil properties. *For. Ecol. Manag.* **2009**, *257*, 1–7. [CrossRef]
75. Hu, H.; Ma, H.; Wang, Y.; Xu, H. Influence of land use types to nutrients, organic carbon and organic nitrogen of soil. *Soill Water Conserv. China* **2010**, *11*, 40–42.
76. Gashaw, T.; Tulu, T.; Argaw, M.; Worqlul, A.W. Evaluation and prediction of land use/land cover changes in the Andassa watershed, Blue Nile Basin, Ethiopia. *Environ. Syst. Res.* **2017**, *6*, 17. [CrossRef]
77. Gebru, B.M.; Lee, W.K.; Khamzina, A.; Lee, S.G.; Negash, E. Hydrological Response of Dry Afromontane Forest to Changes in Land Use and Land Cover in Northern Ethiopia. *Remote Sens.* **2019**, *11*, 1905. [CrossRef]
78. Miheretu, B.A.; Yimer, A.A. Determinants of farmers' adoption of land management practices in Gelana sub-watershed of Northern highlands of Ethiopia. *Ecol. Processes* **2017**, *6*, 19. [CrossRef]
79. Wubie, M.A.; Assen, M.; Nicolau, M.D. Patterns, causes and consequences of land use/cover dynamics in the Gumara watershed of lake Tana basin, Northwestern Ethiopia. *Environ. Syst. Res.* **2016**, *5*, 8. [CrossRef]
80. Li, S.C.; Bing, Z.L.; Jin, G. Spatially Explicit Mapping of Soil Conservation Service in Monetary Units Due to Land Use/Cover Change for the Three Gorges Reservoir Area, China. *Remote Sens.* **2019**, *11*, 468. [CrossRef]
81. Wolka, K.; Tadesse, H.; Garedew, E.; Yimer, F. Soil erosion risk assessment in the Chaleleka wetland watershed, Central Rift Valley of Ethiopia. *Environ. Syst. Res.* **2015**, *4*, 5. [CrossRef]
82. Wijitkosum, S. Impacts of land use changes on soil erosion in Pa Deng sub-district, adjacent area of Kaeng Krachan National Park, Thailand. *Soil Water Res.* **2012**, *7*, 10–17. [CrossRef]
83. Valentin, C.; Agus, F.; Alamban, R.; Boosaner, A.; Bricquet, J.-P.; Chaplot, V.; De Guzman, T.; De Rouw, A.; Janeau, J.-L.; Orange, D. Runoff and sediment losses from 27 upland catchments in Southeast Asia: Impact of rapid land use changes and conservation practices. *Agric. Ecosyst. Environ.* **2008**, *128*, 225–238. [CrossRef]
84. Mekonnen, Z.; Berie, H.T.; Woldeamanuel, T.; Asfaw, Z.; Kassa, H. Land use and land cover changes and the link to land degradation in Arsi Negele district, Central Rift Valley, Ethiopia. *Remote Sens. Appl. Soc. Environ.* **2018**, *12*, 1–9. [CrossRef]